ACS NANO
Cite This: ACS Nano XXXX, XXX, XXX–XXX
www.acsnano.org

ARTICLE

Room-Temperature Electrocaloric Effect in Layered Ferroelectric $CuInP_2S_6$ for Solid-State Refrigeration

Mengwei Si,[†,∥] Atanu K. Saha,[†] Pai-Ying Liao,[†,∥] Shengjie Gao,[‡,∥] Sabine M. Neumayer,[⊥] Jie Jian,[§] Jingkai Qin,[†,∥] Nina Balke Wisinger,[⊥] Haiyan Wang,[§] Petro Maksymovych,[⊥] Wenzhuo Wu,[‡,∥] Sumeet K. Gupta,[†] and Peide D. Ye*[,†,∥]

[†]School of Electrical and Computer Engineering, Purdue University, West Lafayette, Indiana 47907, United States
[‡]School of Industrial Engineering, Purdue University, West Lafayette, Indiana 47907, United States
[§]School of Materials Science and Engineering, Purdue University, West Lafayette, Indiana 47907, United States
[∥]Birck Nanotechnology Center, Purdue University, West Lafayette, Indiana 47907, United States
[⊥]Center for Nanophase Materials Sciences, Oak Ridge National Laboratory, Bethel Valley Road, Oak Ridge, Tennessee 37831, United States

Supporting Information

ABSTRACT: **A material with reversible temperature change capability under an external electric field, known as the electrocaloric effect (ECE), has long been considered as a promising solid-state cooling solution. However, electrocaloric (EC) performance of EC materials generally is not sufficiently high for real cooling applications. As a result, exploring EC materials with high performance is of great interest and importance. Here, we report on the ECE of ferroelectric materials with van der Waals layered structure ($CuInP_2S_6$ or CIPS in this work in particular). Over 60% polarization charge change is observed within a temperature change of only 10 K at Curie temperature. Large adiabatic temperature change ($|\Delta T|$) of 3.3 K and isothermal entropy change ($|\Delta S|$) of 5.8 J kg^{-1} K^{-1} at $|\Delta E|$ = 142.0 kV cm^{-1} and at 315 K (above and near room temperature) are achieved, with a large EC strength ($|\Delta T|/|\Delta E|$) of 29.5 mK cm kV^{-1}. The ECE of CIPS is also investigated theoretically by numerical simulation, and a further EC performance projection is provided.**

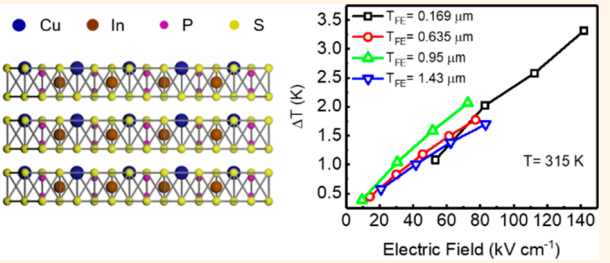

KEYWORDS: *$CuInP_2S_6$, ferroelectrics, electrocaloric effect, two-dimensional, room temperature*

Electrocaloric refrigerators using electrocaloric materials are low noise and environment friendly, and can be scaled down to small dimensions, compared to the common vapor-compression refrigerators.[1−13] Electrocaloric cooling is also much easier and lower in cost to realize compared to other field-induced cooling techniques such as magnetocaloric and mechanocaloric cooling, because the electric field is easily realized and accessible. Thus, electrocaloric effect is promising for future cooling applications, especially in micro- or nanoscale such as on-chip cooling. Electrocaloric effect in ferroelectric materials is of special interest because of the large polarization change near the ferroelectric-paraelectric (FE-PE) phase transition temperature (Curie temperature, T_C). It also defines the working temperature range for such ferroelectric coolers so that above but near room temperature T_C is important for practical applications. Therefore, near Curie temperature as working temperature and adiabatic temperature change ($|\Delta T|$, $|\Delta T|/|\Delta E|$ as EC strength if normalized by electric field) and isothermal entropy change ($|\Delta S|$, $|\Delta S|/|\Delta E|$ if normalized by electric field) are key parameters for the performance of EC materials. One of the key challenges in realizing electrocaloric cooler is the relatively low $|\Delta T|$ and $|\Delta S|$ in current EC materials. The realization of EC cooler requires searching EC materials with high EC performance. Ferroelectric materials with van der Waals layered structure, featured with a van der Waals weak interaction between layers and being easy to form van der Waals heterostructures, may have essential impact on the ferroelectric polarization switching and EC properties because of the different out-of-plane ferroelectric polarization switching process due to the van der Waals gap. Meanwhile, the thermal transport properties of van der Waals layered

Received: February 22, 2019
Accepted: August 2, 2019
Published: August 2, 2019

DOI: 10.1021/acsnano.9b01491
ACS Nano XXXX, XXX, XXX–XXX

materials have strong anisotropicity in in-plane and out-of-plane directions and may provide special properties on heat absorption, heat dissipation, and the design of practical ECE cooling devices. Ferroelectricity in 2D materials has recently started to be studied,[14−17] but is rather rare currently because of the limited research efforts. EC materials with van der Waals heterostructures remain unexplored. Meanwhile, an insulating EC material is also required in a EC refrigerator to avoid Joule heating. $CuInP_2S_6$ (CIPS) has been recently explored as a 2D ferroelectric insulator with T_C about 315 K and switchable polarization down to ∼4 nm.[14,15,18] As a 2D ferroelectric insulator with T_C above but near room temperature, CIPS can be a potential candidate for EC cooling applications.

Here, we report on the ECE on a ferroelectric insulator CIPS with van der Waals layered structure. The T_C at 315 K is only slightly above human body temperature so that the material can have a broad range of practical cooling applications. Over 60% polarization change is observed with a temperature change of only 10 K. A $|\Delta T|$ of 3.3 K and $|\Delta S|$ of 5.8 J kg^{-1} K^{-1} at $|\Delta E|$ = 142.0 kV cm^{-1} and at 315 K are achieved, with a large EC strength ($|\Delta T|/|\Delta E|$) of 29.5 mK cm kV^{-1}. These representative values of CIPS suggest that ferroelectric materials with a van der Waals layered structure can be competitive EC materials and are of great interest to further explore EC materials with van der Waals layered structure for potential applications in microelectronics, bio- or medical sensing, and nanoenergy areas.

RESULTS AND DISCUSSION

CIPS crystals were grown by solid-state reaction.[18,19] Figure 1a shows the crystal structure of CIPS from top- and side-views. It is based on a hexagonal ABC sulfur stacking, which is filled by Cu, In, and P−P pairs and separated by a van der Waals gap. High-angle annular dark field STEM (HAADF-STEM) image of thin CIPS flake is shown in Figure 1b. Distinct arrangement of atoms could be clearly identified, with the fringe space of (100) planes measured to be 0.57 nm. The corresponding selected area electron diffraction (SAED, at a 600 nm by 600 nm region) shows a set of rotational symmetry pattern with perfect hexagonal crystal structure, indicating the CIPS flake is highly single-crystallized (Figure 1b, inset). EDS analysis by SEM on CIPS flakes confirms the $CuInP_2S_6$ stoichiometry.[18] Figure 1c illustrates the Raman spectrum of an exfoliated CIPS thin film from 4 to 325 K. The structure of $CuInP_2S_6$ in the ferroelectric phase is in the space group *Cc*, point group *m*.[19] The primary bands in Raman study are ν(P−S), ν(P−P), ν(S−P−S), and ν(S−P−P) in the 100−500 cm^{-1} range,[20] which shows a dramatic loss in intensity and peak broadening as the temperature is increased from 310 to 315 K, as shown in Figure 1d for a particular example at 373.8 cm^{-1}. Such measurements were repeated on multiple CIPS flakes and show similar loss in intensity and peak broadening at 315 K. Thus, temperature-dependent Raman measurements confirm a structural phase transition in CIPS at 315 K.

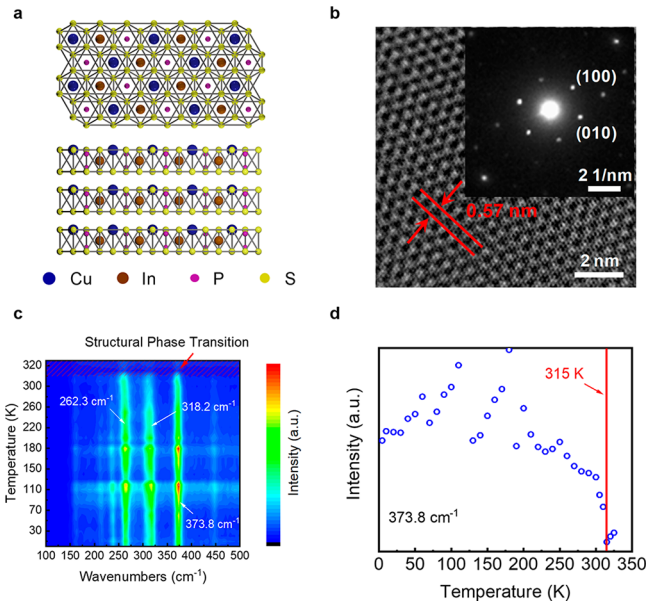

Figure 1. (a) Top- and side-views of CIPS, showing an ABC sulfur stacking, filled by Cu, In, and P−P pairs and separated by a van der Waals gap as a ferroelectric insulator with van der Waals layered structure. (b) HAADF-STEM image of thin CIPS flake viewed along [001] axis and the corresponding SAED pattern. (c) Temperature-dependent Raman spectroscopy on CIPS thin film. (d) Temperature-dependent Raman peak intensity at 373.8 cm^{-1}, showing a large decrease in Raman intensity at 315 K.

Temperature-dependent piezo-response force microscopy (PFM) was studied to investigate the ferroelectricity in CIPS. Figure 2a−c shows the band excitation PFM (BE-PFM) on a fabricated CIPS capacitor using Ni as top and bottom electrodes; the area of the top electrode is 2 μm by 2 μm. Figure 2a shows the BE-PFM images on an as-fabricated CIPS device, both up and down polarization can be observed in PFM phase image, indicating the as-fabricated CIPS device has multidomains. DC voltage pulses of 1 s and ±6 V were then applied to the device to switch the polarization electrically. Clear phase transition can be observed after DC voltage pulses, suggesting a switchable polarization in the fabricated CIPS capacitor, as shown in the different phases (indicating different polarization directions) in Figure 2b,c. The temperature-dependent ferroelectricity was further characterized by dual AC resonance tracking piezo-response force microscopy (DART-PFM). The DART-PFM phase/amplitude images and raw data of single-point hysteresis loop measurements can be found in the Supporting Information, section 1. The phase and amplitude hysteresis loops were achieved by the DART-PFM at a single point in tapping mode. Figure 2d,e shows the phase and amplitude *versus* voltage hysteresis loop of a 0.23 μm-thick CIPS flake on a $Ni/SiO_2/Si$ substrate at 305 K, showing clear ferroelectric polarization switching under an external electric field (PFM phase change of ∼180°). A 90 nm SiO_2 is used in between Ni and Si for better visibility of CIPS flakes. Figure 2f shows the temperature-dependent DART-PFM phase hysteresis loop of the same CIPS flake at 300−325 K. Clear ferroelectric PFM hysteresis loops with distinct polarization switching are achieved at 300−310 K (see also Figure S2), while no obvious phase change can be observed at and above 315 K (see also Figure S3). The loss of ferroelectric phase transition from PFM measurement at and above 315 K directly confirms that CIPS has a Curie temperature of ∼315 K.

The electrical characteristics of CIPS devices were measured using a Ni/CIPS/Ni capacitor on top of a 90 nm SiO_2/Si substrate. The detailed fabrication process can be found in Methods section. Polarization−voltage (*P*−*V*) measurement is used to further investigate the ferroelectric and electrocaloric properties in CIPS. The voltage-dependent *P*−*V* characteristics

DOI: 10.1021/acsnano.9b01491
ACS Nano XXXX, XXX, XXX−XXX

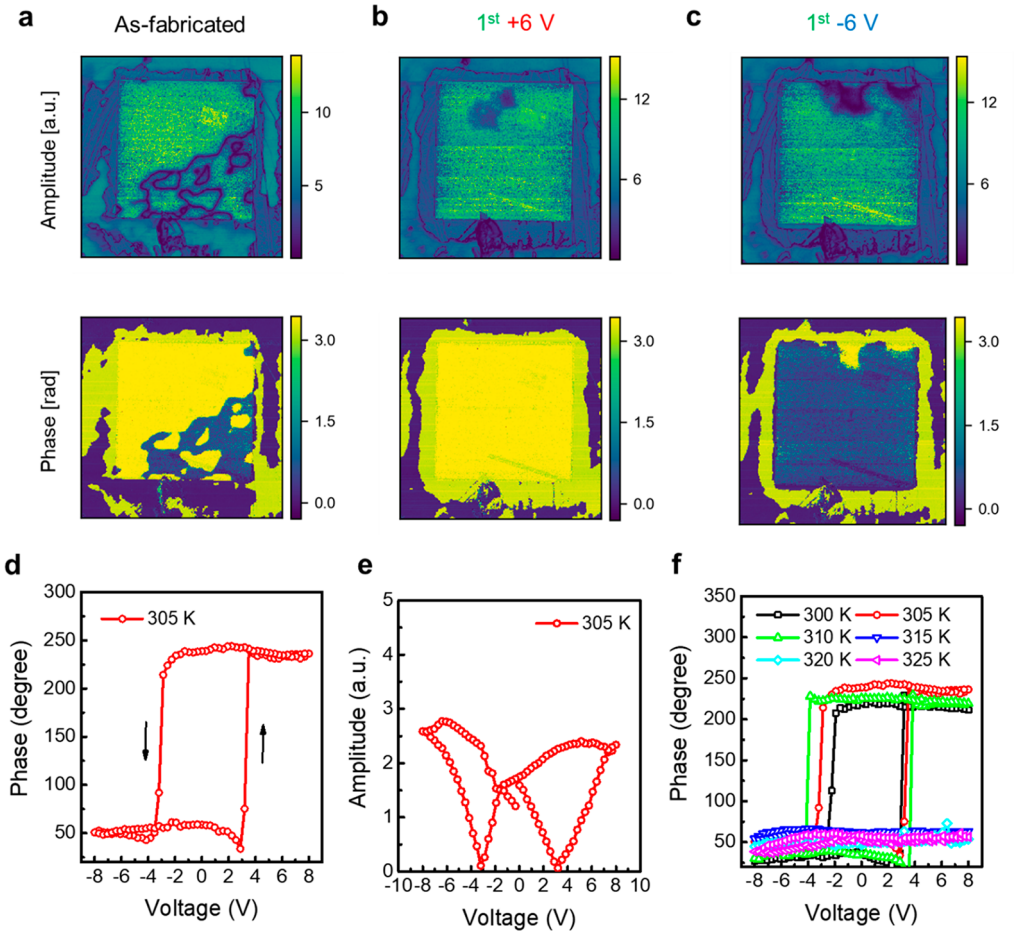

Figure 2. (a) BE-PFM amplitude and phase of as-fabricated CIPS capacitor with 20 nm Ni as top electrode on a Ni/SiO_2/Si substrate, measured at room temperature. The area of the top electrode is 2 μm × 2 μm. (b) BE-PFM amplitude and phase of the same device after 6 V voltage pulse for 1 s. (c) BE-PFM amplitude and phase of the same device after −6 V voltage pulse for 1 s. Stable polarization switching is achieved upon application of DC voltage pulses of 1 s duration and ±6 V amplitude. (d) Phase and (e) amplitude *versus* voltage by DART-PFM hysteresis loop of a 0.23 μm-thick CIPS flake without 20 nm Ni top electrode on a Ni/SiO_2/Si substrate at 305 K, showing clear ferroelectric polarization switching under external electric field. (f) Temperature-dependent DART-PFM phase hysteresis loop of the same CIPS flake at 300−325 K. The loss of ferroelectric phase transition since 315 K, suggesting a ferroelectric Curie temperature of 315 K.

show a stable coercive voltage (V_c) *versus* sweep voltage ranges, as shown in Supporting Information, section 2, suggesting the fabricated CIPS capacitor is highly single-crystallized, which is consistent with the TEM results in Figure 1b. Figure 3a shows the $P-V$ measurement on a CIPS capacitor with CIPS thickness (T_{FE}) of 0.95 μm at temperature from 290 to 330 K in 5 K step, across the Curie temperature of 315 K. A monotonic decrease of polarization *versus* temperature is observed with a peak reduction at 315 K, as shown in Figure 3b, confirms the ferroelectric to paraelectric transition is at 315 K, which is consistent with temperature-dependent Raman spectroscopy and PFM measurements. Note that a fast over 60% polarization change is obtained within only 10 K temperature change, which may be related with the van der Waals layered structure in CIPS. The electrocaloric effect in CIPS is evaluated by indirect method.[6,21] ΔT can be calculated as $-\int_{E_1}^{E_2} \frac{1}{C\rho} T\left(\frac{\partial P}{\partial T}\right)_E dE$, where C is the heat capacity and ρ is density. ΔS can be further calculated as $\int_{E_1}^{E_2} \frac{1}{\rho}\left(\frac{\partial P}{\partial T}\right)_E dE$. As can be seen from the equations of ΔT and ΔS, the fast polarization change with respect to temperature can significantly enhance the EC strength of the EC material. The density of CIPS is 3405 kg m^{-3} at 295 K.[19] The heat capacity of CIPS is 557 J K^{-1} kg^{-1} at 315 K.[22,23] ρ is assumed to have minor change in the temperature range of interest because the experiments were performed in a narrow temperature range between 290 and 330 K. The temperature-dependent heat capacity[23] of CIPS is used in the calculation, although only minor changes happen within the range of interest. Electrocaloric temperature change of the 0.95 μm-thick CIPS is plotted in Figure 3c. A maximum $|\Delta T|$ of 2.0 K is achieved at $|\Delta E|$ of 72.6 kV cm^{-1} (maximum $|\Delta T|/|\Delta E|$ of 29.5 mK cm kV^{-1} and $|\Delta T|/|\Delta V|$ of 0.31 K V^{-1}). The corresponding $|\Delta S|$ *versus* temperature is shown in Figure 3d, with a maximum $|\Delta S|$ of 3.6 J kg^{-1} K^{-1} at $|\Delta E|$ of 72.6 kV cm^{-1}. It is worth noting that the absolute value of remnant polarization of CIPS thin film (~0.03−0.04 C m^{-2}) is rather small (about 1 order of magnitude smaller than common ferroelectric ceramics or ferroelectric polymers). The slope of polarization percentage change with respect to temperature is actually quite high (Supporting Information, section 4). If this is the intrinsic property of ferroelectric materials with van der Waals layered structure, then it is possible to find a high-performance 2D ferroelectric material with high remnant polarization and high EC strength. Thus, ferroelectric materials

DOI: 10.1021/acsnano.9b01491
ACS Nano XXXX, XXX, XXX−XXX

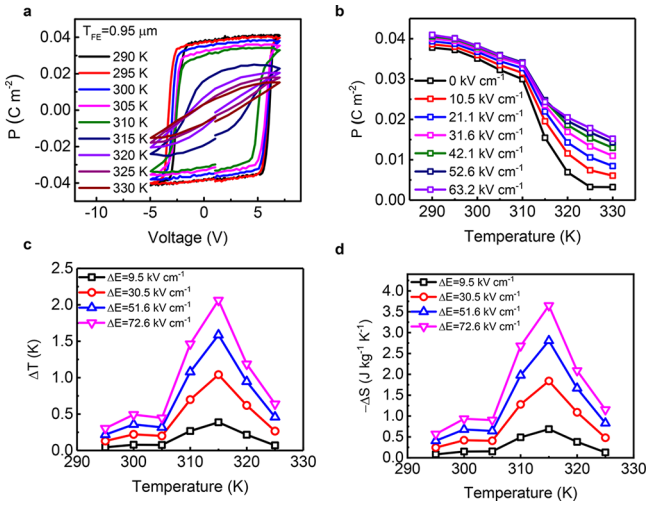

Figure 3. (a) Polarization *versus* voltage characteristics measured at different temperatures of a CIPS capacitor with CIPS thickness of 0.95 μm. (b) Polarization *versus* temperature at different voltage biases, extracted from (a). (c) Adiabatic temperature change |Δ*T*| *versus* temperature at different |Δ*E*|. A maximum |Δ*T*| of 2.0 K is achieved at |Δ*E*| of 72.6 kV cm^{-1} and |Δ*V*| of 6.9 V (maximum |Δ*T*|/|Δ*E*| of 29.5 mK cm kV^{-1} and |Δ*T*|/|Δ*V*| of 0.31 K V^{-1}). (d) Isothermal entropy change |Δ*S*| *versus* temperature at different |Δ*E*|, with a maximum |Δ*S*| of 3.6 J kg^{-1} K^{-1} at |Δ*E*| of 72.6 kV cm^{-1}.

with van der Waals layered structure can be competitive EC materials and of great interest to explore.

Figure 4 investigates the thickness dependence of ECE in CIPS. Figure 4a shows the adiabatic temperature change *versus* temperature characteristics of CIPS capacitors with a CIPS thickness of 0.169 μm. A maximum |Δ*T*| of 3.3 K and a maximum |Δ*S*| of 5.8 J kg^{-1} K^{-1} are achieved at |Δ*E*| of 142.0 kV cm^{-1} in the CIPS capacitor with 0.169 μm thickness. Note that the enhancement of |Δ*T*| and |Δ*S*| is because thinner CIPS films can support a higher electric field. It is also consistent with a previous report that thinner CIPS has a larger coercive electric field.[15] As shown in Figure 4b, adiabatic temperature change |Δ*T*| *versus* electric field |Δ*E*| of CIPS capacitors at 315 K with different CIPS thicknesses from 0.169 to 1.43 μm. The slope as the actual EC strength is not improved in deep sub-μm range thin films. Figure 4c shows the thickness dependence of EC strength in CIPS at 315 K. |Δ*T*|/|Δ*E*| shows minor thickness dependence, while the |Δ*T*|/|Δ*V*| (Figure 4d) is inversely proportional to the thickness as expected. A maximum |Δ*T*|/|Δ*V*| of 1.18 K V^{-1} is obtained on a capacitor with 0.169 μm CIPS and at a |Δ*E*| of 70 kV cm^{-1}. Under electrical breakdown strength, ferroelectric materials with van der Waals layered structure, which have the potential to offer atomically thin films, can realize large |Δ*T*| change by applying very small |Δ*V*|. The required large heat capacity can be realized by integration of a large number of such nanocoolers or nanorefrigerators. However, the leakage current in ultrathin CIPS films at elevated temperatures prevents us from reliably measuring the *P*−*V* hysteresis loop and studying the ECE effect. The undesired leakage current might also provide a joule heating effect so that ultrathin CIPS film is not suitable for real cooling applications.

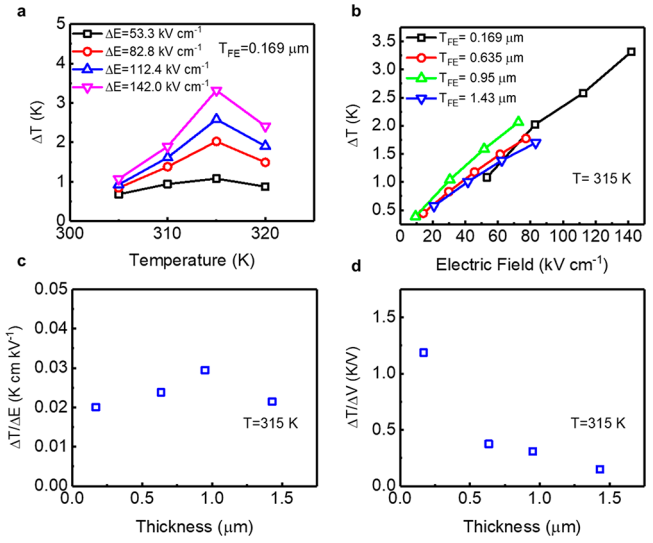

Figure 4. (a) Adiabatic temperature change |Δ*T*| *versus* temperature at different |Δ*E*| of a CIPS capacitor with CIPS thickness of 0.169 μm. A maximum |Δ*T*| of 3.3 K and a maximum |Δ*S*| of 5.8 J kg^{-1} K^{-1} are achieved at |Δ*E*| of 142.0 kV cm^{-1}. (b) Adiabatic temperature change |Δ*T*| *versus* electric field |Δ*E*| of CIPS capacitors with different CIPS thicknesses. (c) Electrocaloric strength |Δ*T*|/|Δ*E*| of CIPS capacitors with different CIPS thicknesses. (d) Normalized adiabatic temperature change with respect to voltage of CIPS capacitors with different CIPS thicknesses.

Furthermore, the EC effects in CIPS are theoretically investigated by numerical simulations. The Landau−Khalatnikov equation is solved by calibrating the Landau coefficients with experimentally measured remnant polarization (P_r = ~0.04 C m^{-2}) and coercive field (E_C = ~60 kV cm^{-1}) of CIPS at T = 295 K. Note that the measured temperature-dependent *P*−*V* curves (Figure 3a) show an abrupt phase transition near T = 315 K. Detailed simulation methods and parameters can be found in Supporting Information, section 3. Considering the second-order phase transition with a Curie−Weiss temperature, T_0 (or T_C) of 315 K, the simulated temperature-dependent *P*−*V* characteristics are shown in Figure 5a. Similarly, the simulated polarization *versus* temperature characteristics are plotted in Figure 5b. To evaluate the EC effects, |Δ*T*| at different temperatures are calculated for different |Δ*E*| from 0 to 100 kV cm^{-1} (using same method as in Figure 3) and is shown in Figure 5c. The simulation results (Figure 5a−c) show good agreement with the experimental results (Figure 3c) and suggest that in the case of second-order phase transition, maximum EC temperature change occurs at 315 K. In contrast to the second-order phase transition, a class of FE materials (such as BTO)[24−26] exhibit a two-step hysteresis loop change, first from a single hysteresis loop to double hysteresis loop and then from a double hysteresis loop to PE hysteresis loop. Figure 5d shows the impact of remnant polarization on the EC performance of ferroelectric materials. It can be clearly seen that EC strength is higher with higher P_r. Thus, a ferroelectric material with high remnant polarization with T_c above but near room temperature is preferred for high-performance EC applications.

CONCLUSION

In conclusion, the electrocaloric effect on a ferroelectric material with van der Waals layered structure is investigated. Over 60% polarization change is observed with a temperature change of 10 K in CIPS. A |Δ*T*| of 3.3 K and |Δ*S*| of 5.8 J kg^{-1}

DOI: 10.1021/acsnano.9b01491
ACS Nano XXXX, XXX, XXX−XXX

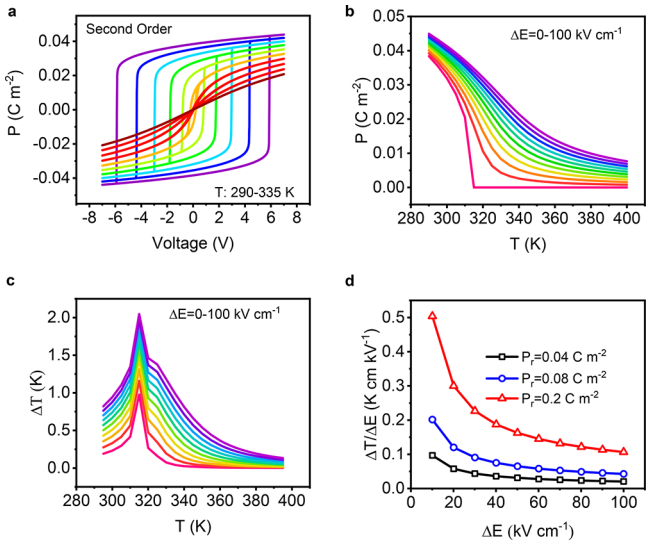

Figure 5. (a) Polarization *versus* voltage characteristics considering second-order phase transition at temperature from 290 to 335 K in 5 K step. (b) Polarization *versus* temperature at different voltage biases, extracted from (a). (c) EC temperature change $|\Delta T|$ *versus* temperature at different $|\Delta E|$. (d) The impact of remnant polarization on EC strength.

K^{-1} at $|\Delta E|$ = 142.0 kV cm^{-1} and at 315 K are achieved, with a large EC strength ($|\Delta T|/|\Delta E|$) of 29.5 mK cm kV^{-1}. The EC effect of CIPS is also investigated theoretically by numerical simulation, and a further EC performance projection is provided. These results suggest the investigation of electrocaloric effects in ferroelectric materials with van der Waals layered structure is of great interest and importance for microelectronics, sensing, and nanoenergy applications.

METHODS

$CuInP_2S_6$ Growth. CIPS crystals were grown by solid-state reaction. Powders of the four elements were mixed and placed in an ampule with the same ratio of the stoichiometry (246 mg of Cu, 441 mg of In, 244 mg of P, and 752 mg of S). The ampule was heated in vacuum at 600 °C for 2 weeks to obtain the CIPS crystals.

Device Fabrication. CIPS flakes were transferred to the 20 nm Ni/90 nm SiO_2/p+ Si substrate by scotch tape-based mechanical exfoliation. A top electrode using 20 nm nickel and gold was fabricated using electron-beam lithography, electron-beam evaporation, and lift-off process.

Material Characterization. The HAADF-STEM was performed with FEI Talos F200x equipped with a probe corrector. This microscope was operated with an acceleration voltage of 200 kV. DART-PFM was carried out on Asylum Cypher ES, and the conductive AFM tip has averaged spring constant ~5 N/m. Temperature-dependent Raman measurement was done with Montana Instruments S100-CO with a 100× 0.75NA objective integrated with a Princeton Instruments FERGIE spectrometer using a 1200 g/mm grating blazed at 550 nm. A single mode fiber coupled 532 nm laser with a <1 MHz bandwidth was used as the excitation source.

Device Characterization. The thickness of the CIPS device was measured using a Veeco Dimension 3100 AFM or a KLA-Tencor Alpha-Step IQ. DC electrical characterization was performed with a Keysight B1500 system. Temperature-dependent electrical data were collected with a Cascade Summit probe station.

ASSOCIATED CONTENT

Supporting Information

The Supporting Information is available free of charge on the ACS Publications website at DOI: 10.1021/acsnano.9b01491.

Additional details for DART-PFM measurement (raw data, temperature dependence, and thickness dependence) on CIPS, voltage-dependent $P-V$ measurement, ECE simulation method, and benchmarking of EC materials (PDF)

AUTHOR INFORMATION

Corresponding Author

*E-mail: yep@purdue.edu.

ORCID

Mengwei Si: 0000-0003-0397-7741
Sabine M. Neumayer: 0000-0002-8167-1230
Nina Balke Wisinger: 0000-0001-5865-5892
Haiyan Wang: 0000-0002-7397-1209
Wenzhuo Wu: 0000-0003-0362-6650
Peide D. Ye: 0000-0001-8466-9745

Author Contributions

P.Y.L. synthesized the $CuInP_2S_6$. M.S. did the device fabrication, electrical measurement, and analysis. S.G., M.S., and W.W. measured the temperature-dependent DART-PFM. S.M.N., N.B., and P.M. performed the BE-PFM measurement. J.Q., J.J., and H.W. conducted the TEM and EDS measurements. A.K.S. and S.K.G. did the numerical simulation. M.S and P.D.Y. summarized the manuscript, and all authors commented on it.

Notes

This manuscript has been authored by UT-Battelle, LLC, under contract no. DEAC0500OR22725 with the U.S. Department of Energy. The United States Government retains and the publisher, by accepting the article for publication, acknowledges that the United States Government retains a non-exclusive, paid-up, irrevocable, world-wide license to publish or reproduce the published form of this manuscript or allow others to do so, for the United States Government purposes. The Department of Energy will provide public access to these results of federally sponsored research in accordance with the DOE Public Access Plan (http://energy.gov/downloads/doe-public-access-plan).

The authors declare no competing financial interest.

ACKNOWLEDGMENTS

This material is based upon work partly supported by the Semiconductor Research Corporation (SRC) and DARPA. J.J. and H.W. acknowledge the support from the U.S. Office of Naval Research (N00014-16-1-2465) for the TEM effort. PFM measurements were supported by the Division of Materials Science and Engineering, Basic Energy Sciences, US Department of Energy. BE-PFM experiments were conducted at the Center for Nanophase Materials Sciences, which is a DOE Office of Science User Facility. The authors gratefully acknowledge C. Wall and Montana Instruments for technical support on the temperature-dependent Raman characterization. The authors would also like to thank V. Liubachko and Y. M. Vysochanskii for identifying the heat capacity of $CuInP_2S_6$ and valuable discussions.

DOI: 10.1021/acsnano.9b01491
ACS Nano XXXX, XXX, XXX−XXX

REFERENCES

(1) Mischenko, A. S.; Zhang, Q.; Scott, J. F.; Whatmore, R. W.; Mathur, N. D. Giant Electrocaloric Effect in Thin-Film $PbZr_{0.95}Ti_{0.05}O_3$. *Science* **2006**, *311*, 1270−1271.

(2) Neese, B.; Chu, B.; Lu, S.-G.; Wang, Y.; Furman, E.; Zhang, Q. M. Large Electrocaloric Effect in Ferroelectric Polymers near Room Temperature. *Science* **2008**, *321*, 821−823.

(3) Lu, S. G.; Rožič, B.; Zhang, Q. M.; Kutnjak, Z.; Li, X.; Furman, E.; Gorny, L. J.; Lin, M.; Malič, B.; Kosec, M.; Blinc, R.; Pirc, R. Organic and Inorganic Relaxor Ferroelectrics with Giant Electrocaloric Effect. *Appl. Phys. Lett.* **2010**, *97*, 162904.

(4) Scott, J. F. Electrocaloric Materials. *Annu. Rev. Mater. Res.* **2011**, *41*, 229−240.

(5) Valant, M. Electrocaloric Materials for Future Solid-State Refrigeration Technologies. *Prog. Mater. Sci.* **2012**, *57*, 980−1009.

(6) Moya, X.; Kar-Narayan, S.; Mathur, N. D. Caloric Materials near Ferroic Phase Transitions. *Nat. Mater.* **2014**, *13*, 439−450.

(7) Qian, X.-S.; Ye, H.-J.; Zhang, Y.-T.; Gu, H.; Li, X.; Randall, C. A.; Zhang, Q. M. Giant Electrocaloric Response over a Broad Temperature Range in Modified $BaTiO_3$ Ceramics. *Adv. Funct. Mater.* **2014**, *24*, 1300−1305.

(8) Zhang, G.; Li, Q.; Gu, H.; Jiang, S.; Han, K.; Gadinski, M. R.; Haque, M. A.; Zhang, Q.; Wang, Q. Ferroelectric Polymer Nanocomposites for Room-Temperature Electrocaloric Refrigeration. *Adv. Mater.* **2015**, *27*, 1450−1454.

(9) Liu, Y.; Scott, J. F.; Dkhil, B. Direct and Indirect Measurements on Electrocaloric Effect: Recent Developments and Perspectives. *Appl. Phys. Rev.* **2016**, *3*, 031102.

(10) Ma, R.; Zhang, Z.; Tong, K.; Huber, D.; Kornbluh, R.; Ju, Y. S.; Pei, Q. Highly Efficient Electrocaloric Cooling with Electrostatic Actuation. *Science* **2017**, *357*, 1130−1134.

(11) Lu, B.; Li, P.; Tang, Z.; Yao, Y.; Gao, X.; Kleemann, W.; Lu, S.-G. Large Electrocaloric Effect in Relaxor Ferroelectric and Antiferroelectric Lanthanum Doped Lead Zirconate Titanate Ceramics. *Sci. Rep.* **2017**, *7*, 45335.

(12) Jian, X.-D.; Lu, B.; Li, D.-D.; Yao, Y.-B.; Tao, T.; Liang, B.; Guo, J.-H.; Zeng, Y.-J.; Chen, J.-L.; Lu, S.-G. Direct Measurement of Large Electrocaloric Effect in $Ba(Zr_xTi_{1-x})O_3$ Ceramics. *ACS Appl. Mater. Interfaces* **2018**, *10*, 4801−4807.

(13) Lu, B.; Yao, Y.; Jian, X.; Tao, T.; Liang, B.; Zhang, Q. M.; Lu, S.-G. Enhancement of the Electrocaloric Effect over a Wide Temperature Range in PLZT Ceramics by Doping with Gd^{3+} and Sn^{4+} Ions. *J. Eur. Ceram. Soc.* **2019**, *39*, 1093−1102.

(14) Belianinov, A.; He, Q.; Dziaugys, A.; Maksymovych, P.; Eliseev, E.; Borisevich, A.; Morozovska, A.; Banys, J.; Vysochanskii, Y.; Kalinin, S. V. $CuInP_2S_6$ Room Temperature Layered Ferroelectric. *Nano Lett.* **2015**, *15*, 3808−3814.

(15) Liu, F.; You, L.; Seyler, K. L.; Li, X.; Yu, P.; Lin, J.; Wang, X.; Zhou, J.; Wang, H.; He, H.; Pantelides, S. T.; Zhou, W.; Sharma, P.; Xu, X.; Ajayan, P. M.; Wang, J.; Liu, Z. Room-Temperature Ferroelectricity in $CuInP_2S_6$ Ultrathin Flakes. *Nat. Commun.* **2016**, *7*, 12357.

(16) Zhou, Y.; Wu, D.; Zhu, Y.; Cho, Y.; He, Q.; Yang, X.; Herrera, K.; Chu, Z.; Han, Y.; Downer, M. C.; Peng, H.; Lai, K. Out-of-Plane Piezoelectricity and Ferroelectricity in Layered α-In_2Se_3 Nanoflakes. *Nano Lett.* **2017**, *17*, 5508−5513.

(17) Fei, Z.; Zhao, W.; Palomaki, T. A.; Sun, B.; Miller, M. K.; Zhao, Z.; Yan, J.; Xu, X.; Cobden, D. H. Ferroelectric Switching of a Two-Dimensional Metal. *Nature* **2018**, *560*, 336−339.

(18) Si, M.; Liao, P. Y.; Qiu, G.; Duan, Y.; Ye, P. D. Ferroelectric Field-Effect Transistors Based on MoS_2 and $CuInP_2S_6$ Two-Dimensional van der Waals Heterostructure. *ACS Nano* **2018**, *12*, 6700−6705.

(19) Maisonneuve, V.; Evain, M.; Payen, C.; Cajipe, V. B.; Molinié, P. Room-Temperature Crystal Structure of the Layered Phase $Cu^{I}In^{III}P_2S_6$. *J. Alloys Compd.* **1995**, *218*, 157−164.

(20) Vysochanskii, Y. M.; Stephanovich, V.; Molnar, A.; Cajipe, V.; Bourdon, X. Raman Spectroscopy Study of the Ferrielectric-Paraelectric Transition in Layered $CuInP_2S_6$. *Phys. Rev. B: Condens. Matter Mater. Phys.* **1998**, *58*, 9119−9124.

(21) Tuttle, B. A.; Payne, D. A. The Effects Of Microstructure On The Electrocaloric Properties Of $Pb(Zr,Sn,Ti)O_3$ Ceramics. *Ferroelectrics* **1981**, *37*, 603−606.

(22) Liubachko, V.; Shvalya, V.; Oleaga, A.; Salazar, A.; Kohutych, A.; Pogodin, A.; Vysochanskii, Y. M. Anisotropic Thermal Properties and Ferroelectric Phase Transitions in Layered $CuInP_2S_6$ and $CuInP_2Se_6$ Crystals. *J. Phys. Chem. Solids* **2017**, *111*, 324−327.

(23) Beley, L. M. Thermodynamic Properties of Ferroelectric Crystals $CuInP_2(Se_x, S_{1-x})_6$. *Ph.D. Thesis*, Uzhhorod National University, 2007.

(24) Cross, L. E. CXXIII. The Dielectric Properties of Barium Titanate Single Crystals in the Region of Their Upper Transition Temperature. *London, Edinburgh, and Dublin Philosophical Magazine and Journal of Science* **1953**, *44*, 1161−1170.

(25) Merz, W. J. Double Hysteresis Loop of $BaTiO_3$ at the Curie Point. *Phys. Rev.* **1953**, *91*, 513−517.

(26) Drougard, M. E. Discontinuous Field-Induced Transitions in Barium Titanate above the Curie Point. *J. Appl. Phys.* **1956**, *27*, 1559−1560.

DOI: 10.1021/acsnano.9b01491
ACS Nano XXXX, XXX, XXX−XXX